Josephson current through a correlated quantum level: Andreev states and π junction behavior

E. Vecino, A. Martín-Rodero, and A. Levy Yeyati
Departamento de Física Teórica de la Materia Condensada C-V, Universidad Autónoma de Madrid, E-28049 Madrid, Spain
(Received 13 December 2002; revised manuscript received 7 March 2003; published 10 July 2003)

The Josephson transport and the electronic properties of a quantum dot characterized by a single level coupled to superconducting leads is analyzed. Different approximations are used and compared: the mean-field approximation, the second-order perturbation theory in the Coulomb interaction, and the exact diagonalization in the zero bandwidth limit. The system exhibits a rich behavior as a function of the relevant parameters. We discuss in detail the conditions for the observation of π junction behavior and the effect of Coulomb interactions on the Andreev states.

DOI: 10.1103/PhysRevB.68.035105 PACS number(s): 74.50.+r

I. INTRODUCTION

The observation of the Kondo effect in semiconducting quantum dots[1] has opened a new area of research in which electronic transport through a nanoscale strongly correlated system can be studied under controlled conditions. More recently, this effect has also been observed in carbon nanotubes coupled to metallic electrodes, a system that can behave in many respects as a quantum dot.[2] These type of devices provide an almost ideal system to test different theoretical predictions. In this direction, great theoretical interest has arisen in connection with the possibility of replacing the normal electrodes by superconducting ones. In fact, carbon nanotubes connected to superconducting leads, that are already being produced, can provide a physical realization of such a system.[3]

In these types of systems an issue of fundamental relevance is the interplay between electron correlation effects and Andreev reflection processes, which provide the basic mechanism for transport between normal and superconducting regions. This interplay has been analyzed by several authors for the case of a quantum dot coupled to a normal and superconducting electrode.[4,5] There have also been some works addressing the problem of the electron transport mediated by multiple Andreev reflections through a resonant level between two superconducting electrodes.[6]

When both electrodes are superconducting a more basic question is how the electron-electron interactions in the dot would affect the Josephson current. This issue has received considerable attention in recent years.[7–11] In particular, the discussion has been centered to a large extent around the appearance of a π-junction behavior induced by electron-electron interactions. The π-junction behavior, which consists in a reversal of the sign of the supercurrent under certain conditions, was first pointed out by Kulik[12] when analyzing the Josephson tunneling in the presence of magnetic impurities, and discussed afterwards by several authors.[13–15] This issue is also related to the interplay between superconductivity and magnetism. π-junction behavior has in fact been recently observed in *S-F-S* Josephson junctions.[16]

The existing theoretical works analyzing the Josephson effect in a single correlated level coupled to superconducting leads have adopted either a mean field description[8] or are restricted to some limiting situations.[7,9] In Ref. 7 the current was obtained to the lowest order in the tunneling coupling, thereby neglecting the important physics associated with the Andreev bound states. On the other hand, in Refs. 9,10 the limit of infinite Coulomb repulsion was considered.

At this point we believe that further work is needed to understand the physical behavior of this system for a broad parameter range. This behavior is actually rather complex due to the several energy scales involved. In particular, as the Andreev bound states play a crucial role in the transport properties, a detailed analysis of electron correlation effects on these states seems desirable. In this paper we present a theoretical study of the Josephson effect in a single level quantum dot coupled to superconducting electrodes. Different approaches are considered. We first study the zero bandwidth limit in which the problem can be exactly diagonalized. Then, as an approximation to the full model we use a diagrammatic expansion of the self-energy associated with the Coulomb interaction in which the coupling to the superconducting leads is taken into account up to infinite order. This last ingredient is important for a proper description of the Andreev bound states.

In Sec. II, we introduce the theoretical model and discuss the diagrammatic approximations for the electron self-energy. In Sec. III we present a simplified version of this model in which the Coulomb interaction is replaced by an effective exchange field. This simple model already describes the π-junction transition and allows us to understand the behavior of the Andreev states under a finite magnetization in the dot. Section IV is devoted to the analysis of the zero bandwidth limit in which the model becomes equivalent to a finite system which can be solved exactly. The exact solution is then used as a test of the approximations used for the electron self-energy. It turns out that the zero bandwidth limit can describe rather accurately most of the properties of the full model. The results for the full model are presented in Sec. V. We first discuss two opposite limiting situations in which the coupling of the dot to the leads is either small or large compared to the superconducting gap. As in the zero bandwidth limit, in the case of weak coupling we show that the problem can be solved exactly. We also present some numerical results for the intermediate regime. The paper is closed by a brief summary of the main conclusions.

II. MODEL AND THEORETICAL APPROACH

We describe a small quantum dot connected to superconducting electrodes by means of a modified single-level Anderson model, given by

$$\hat{H}=\hat{H}_L+\hat{H}_R+\sum_{\sigma}\ \epsilon_0\hat{n}_\sigma+U\hat{n}_\uparrow\hat{n}_\downarrow+\hat{H}_T, \tag{1}$$

where $\hat{n}_\sigma=\hat{c}^\dagger_{0\sigma}\hat{c}_{0\sigma}$, $\hat{H}_L$ and $\hat{H}_R$ represent the uncoupled superconducting leads; $\hat{H}_T=\Sigma_{k\in L,R;\sigma}t_{0,k}\hat{c}^\dagger_{0\sigma}\hat{c}_{k,\sigma}+\text{H.c.}$ describing the coupling between the dot level and the leads. Within this model the dot is represented by a single spin degenerate level with a repulsive Coulomb interaction described by the U term in Eq. (1). We shall assume that the superconducting leads are well described by the BCS theory with a superconducting gap Δ and that there is a fixed superconducting phase difference $\phi=\phi_L-\phi_R$ between both electrodes. It is interesting to have an estimate of the typical values that the model parameters can adopt in an actual experimental situation. Thus, for instance, in the experiments on carbon nanotubes of Ref. 3, $U\approx 0.45$ meV and $\Delta\approx 0.1$ meV. On the other hand the coupling to the leads vary from sample to sample which allows to study the transition from weak to strong coupling.

The relevant quantities such as the current and the spectral densities can be expressed in terms of nonequilibrium Green functions.[17] For the description of the superconducting state it is useful to introduce spinor field operators,[18] which in a site representation are defined as:

$$\hat{\psi}_i=\begin{pmatrix} c_{i\uparrow} \\ c^\dagger_{i\downarrow}\end{pmatrix},\quad \hat{\psi}^\dagger_i=(c^\dagger_{i\uparrow}\quad c_{i\downarrow}). \tag{2}$$

Then, the different correlation functions appearing in the Keldysh formalism adopt the standard causal form

$$\hat{G}^{\alpha,\beta}_{ij}(t_\alpha,t'_\beta)=-i\langle\hat{T}[\hat{\psi}_i(t_\alpha)\hat{\psi}^\dagger_i(t'_\beta)]\rangle, \tag{3}$$

where $\hat{T}$ is the chronological ordering operator along the Keldysh time contour. The labels α and β refer to the upper ($\alpha\equiv+$) and lower ($\alpha\equiv-$) branches on this contour. The functions $\hat{G}^{+-}_{ij}$, which can be associated within this formalism with the electronic nonequilibrium distribution functions, are given by the (2×2) matrix

$$\hat{G}^{+-}_{i,j}(t,t')=i\begin{pmatrix}\langle c^\dagger_{j\uparrow}(t')c_{i\uparrow}(t)\rangle & \langle c_{j\downarrow}(t')c_{i\uparrow}(t)\rangle \\ \langle c^\dagger_{j\uparrow}(t')c^\dagger_{i\downarrow}(t)\rangle & \langle c_{j\downarrow}(t')c^\dagger_{i\downarrow}(t)\rangle\end{pmatrix}. \tag{4}$$

In terms of the Fourier transform matrix elements of $\hat{G}^{+-}_{ij}(t,t')$ one can write the charge and the induced order parameter on the dot, as well as the Josephson current:

$$\langle\hat{n}_\uparrow\rangle=\frac{1}{2\pi i}\int_{-\infty}^{\infty}d\omega[\hat{G}^{+-}_{00}(\omega)]_{11}, \tag{5}$$

$$\langle c^\dagger_{0\uparrow}c^\dagger_{0\downarrow}\rangle=-\frac{1}{2\pi i}\int_{-\infty}^{\infty}d\omega[\hat{G}^{+-}_{00}(\omega)]_{21}, \tag{6}$$

$$I_{L,R}=\frac{e}{h}\int_{-\infty}^{\infty}\sum_{k\in L,R}d\omega\,\mathrm{Tr}[\sigma_z\hat{t}_{0,k}\hat{G}^{+-}_{k,0}(\omega)-\sigma_z\hat{t}_{k,0}\hat{G}^{+-}_{0,k}(\omega)], \tag{7}$$

where $I_{L,(R)}$ denotes the current between the left (right) lead and the dot, σ_z is the usual Pauli matrix, and $\hat{t}_{0,k}$ is the hopping matrix in the Nambu representation

$$\hat{t}_{0,k}=(\hat{t}_{k,0})^\dagger=\begin{pmatrix}t_{0,k} & 0\\ 0 & -t^*_{0,k}\end{pmatrix}. \tag{8}$$

For the zero voltage case the calculation of the different $\hat{G}^{+-}(\omega)$ is particularly simple because the following relation holds:

$$\hat{G}^{+-}_{ij}(\omega)=f(\omega)[\hat{G}^a_{ij}(\omega)-\hat{G}^r_{ij}(\omega)], \tag{9}$$

where $f(\omega)$ is the Fermi distribution function and $\hat{G}^{a,r}$ are the advanced and retarded Green functions. Therefore, the relevant quantity to be determined is the dot retarded Green function, which in the Nambu 2×2 representation adopts the form

$$\hat{G}^r_{00}(\omega)=[\omega\hat{I}-\epsilon_0\hat{\sigma}_z-\hat{\Sigma}^r(\omega)-\hat{\Gamma}_L(\omega)-\hat{\Gamma}_R(\omega)]^{-1}, \tag{10}$$

where $\hat{\Gamma}_{L,R}$ are the tunneling rates given $\hat{\Gamma}_k=\pi\rho_F\hat{t}_{0,k}\hat{g}^k\hat{t}_{k,0}$, with $g^k_{11}=g^k_{22}=-\omega/\sqrt{\Delta^2-\omega^2}$ and $g^k_{12}=(g^k_{21})^*=\Delta/\sqrt{\Delta^2-\omega^2}e^{i\phi_k}$ with $k=L,R$ and where ρ_F is the normal density of states at the Fermi level (the chemical potential of the superconducting leads is taken as zero). The self-energy $\hat{\Sigma}^r(\omega)$ takes into account the effect of Coulomb interactions. To the lowest order in U this is given by the Hartree-Fock Bogoliubov approximation $(\hat{\Sigma}^r)_{11}=U\langle\hat{n}_\downarrow\rangle$, $(\hat{\Sigma}^r)_{22}=-U\langle\hat{n}_\uparrow\rangle$, $(\hat{\Sigma}^r)_{21}=(\hat{\Sigma}^r)^*_{12}=U\langle\hat{c}^\dagger_{0\uparrow}\hat{c}^\dagger_{0\downarrow}\rangle$. We shall discuss in how correlation effects beyond this mean-field approximation can be included in Sec. II.

This model has been analyzed within a mean-field approximation in Ref. 8. In that work the mean field solution was simplified by neglecting the induced order parameter in the dot and imposing self-consistency only in the dot magnetization. However, the complete Hartree-Fock Bogoliubov solution requires the self-consistent determination of both the diagonal and nondiagonal charges in the dot. It should be noticed that the self-consistent determination of the induced complex order parameter is in principle necessary in order to ensure current conservation.[19]

Inclusion of correlation effects. In order to go beyond the mean-field approximation, we consider the diagrammatic expansion of the self-energy in terms of one-electron propagators in Nambu space. In Fig. 1 we show the corresponding second order diagrams in the electron-electron interaction. Due to the appearance of the anomalous propagators G_{12} and G_{21} in the superconducting state, there are additional diagrams to the one contributing in the normal state, labeled by 11(a) in Fig. 1, corresponding to the interaction of a quasiparticle with an electron hole pair with opposite spin.

The proper choice of the unperturbed one-electron Hamiltonian over which the diagrammatic expansion is performed is an important issue. For the normal Anderson model in the symmetric case ($\epsilon_0 = -U/2$) the Hartree approximation which renormalizes the dot level as $\epsilon_0 + U/2$ is the adequate starting point for the perturbation theory as it automatically warrants charge consistency between the perturbed and the unperturbed situation. However, in a nonsymmetric case perturbation over the Hartree field yields pathological results close to half-filling (see Ref. 21). As discussed in Ref. 21 a better choice is to define an effective dot level $\epsilon_{\rm eff}$ in such a way that charge consistency between the effective and the interacting problems is achieved. The natural extension of this scheme to the superconducting case is to impose also consistency in the nondiagonal charge n_{12} by introducing an effective local pairing potential $\Delta_{\rm eff}$ in the unperturbed Hamiltonian.[5]

With these definitions, the dot Green functions in the unperturbed effective problem are given by (hereafter we omit the subscript 00 in the dot Green functions)

$$\hat{G}^{r(0)}(\omega) = \frac{1}{D(\omega)} \begin{pmatrix} \omega - \epsilon_{\rm eff} - t_L^2 g_{11}^L - t_R^2 g_{11}^R & -\Delta_{\rm eff} + t_L^2 g_{12}^L + t_R^2 g_{12}^R \\ -\Delta_{\rm eff}^* + t_L^2 g_{21}^L + t_R^2 g_{21}^R & \omega + \epsilon_{\rm eff} - t_L^2 g_{22}^L - t_R^2 g_{22}^R \end{pmatrix}, \tag{11}$$

where $D(\omega)$ is the corresponding determinant. Notice that the Andreev states in the unperturbed problem are determined by the condition $D(\omega) = 0$, which, in the general case, can have up to four solutions.

The different contributions to the self-energy represented in Fig. 1 can then be written in terms of the one-electron propagators as discussed in the Appendix. The second-order self-energy is in principle valid in the limit $U < \Gamma$. In order to extend its range of validity an ansatz which interpolates correctly between the limits $U/\Gamma \to 0$ and $U/\Gamma \to \infty$ can be used.[5] Within this interpolative approach the matrix self-energy is given by the following expression:[5]

$$\hat{\Sigma}(\omega) = U\langle \hat{n} \rangle \hat{\sigma}_z + \Delta_d \hat{\sigma}_x + [\hat{I} - \alpha \hat{\Sigma}^{(2)} \hat{\sigma}_z]^{-1} \hat{\Sigma}^{(2)}(\omega), \tag{12}$$

where

$$\alpha = \frac{\epsilon_0 + (1 - \langle \hat{n} \rangle) U - \epsilon_{\rm eff}}{U^2 \langle \hat{n} \rangle (1 - \langle \hat{n} \rangle)},$$

and $\hat{\Sigma}^{(2)}$ is the second-order self-energy.

This interpolative scheme has been used in many different contexts involving strongly correlated electrons.[20–22] Notice, however, that for the electron-hole symmetric case the interpolative self-energy reduces to the second-order one. In this case the $U/\Gamma \to \infty$ limit is correctly described by the second-order self-energy except for a narrow region around the Fermi energy.[23] A more precise idea of the validity of the second-order self-energy will be obtained in the comparison with exact results discussed in Sec. IV.

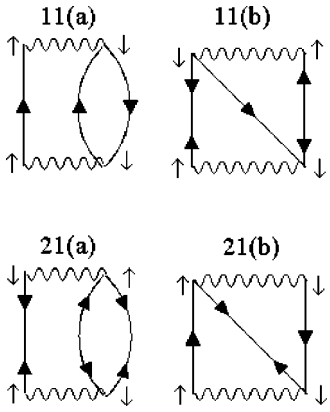

FIG. 1. Diagrams contributing to the second-order self-energy in the superconducting state.

III. TRANSITION FROM NORMAL TO π JUNCTION BEHAVIOR: A SIMPLE MODEL

An exactly solvable model which can describe the transition from normal to π junction behavior is obtained by substituting the interacting region by a single site with a local exchange field $E_{\rm ex}$, in such a way that $\epsilon_\uparrow = \epsilon_0 + E_{\rm ex}$ and $\epsilon_\downarrow = \epsilon_0 - E_{\rm ex}$. It should be noticed that this model is formally equivalent to a mean field solution of Hamiltonian (1) with the prescription $E_{\rm ex} = U(n_\downarrow - n_\uparrow)/2$.

This model exhibits in general four bound states inside the superconducting gap (Andreev states) which give the dominant contribution to the current. This is determined by the derivative of the states below the Fermi energy with respect to the phase. The position and spectral weight of these states can be obtained from the retarded Green function [Eq. (10)]. In the limit $\Delta \ll \Gamma$ and when $\Gamma_L = \Gamma_R = \Gamma$, the Andreev states can be determined analytically by the expression

$$\left(\frac{\omega_\pm}{\Delta} \right)^2 = \frac{\cos^2\phi/2 + 2E^2 + Z^2(Z^2 + \sin^2\phi/2) \pm 2XS(\phi)}{Z^4 + 2(X^2 + E^2) + 1}, \tag{13}$$

where $E = \epsilon_0/2\Gamma$, $X = E_{\rm ex}/2\Gamma$, and $Z^2 = X^2 - E^2$ and $S(\phi)$ is given by

$$S(\phi) = \sqrt{Z^2 \cos^2\phi/2 + E^2 + (\sin^2\phi)/4}.$$

It can be verified that in the limit $X \to 0$ Eq. (13) recovers the well known expression for the Andreev states in a single channel contact of transmission $\tau = 1/(1 + E^2)$, i.e., $\omega/\Delta = \pm\sqrt{1 - \tau \sin^2\phi/2}$.[24]

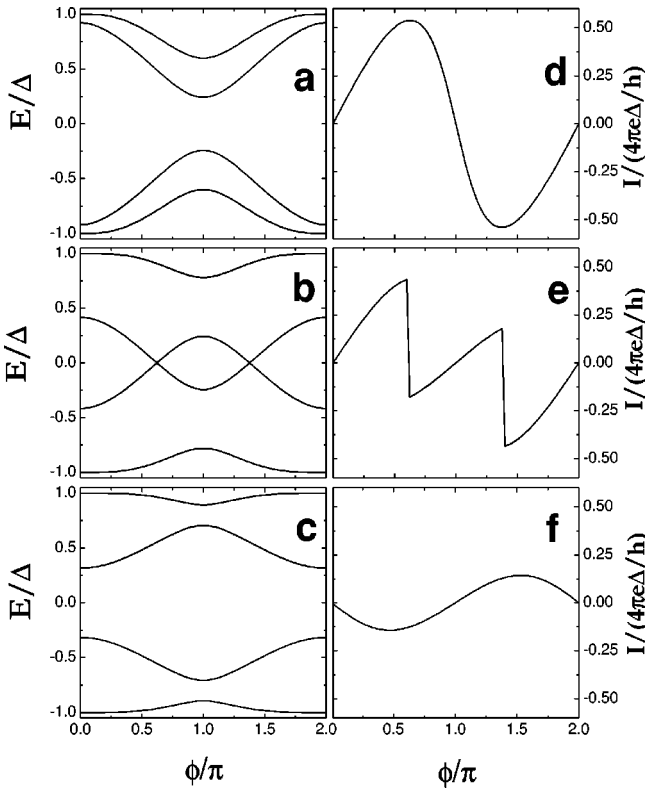

FIG. 2. Bound states within the energy gap and current-phase relation for the simple model discussed in Sec. III. For $\epsilon_0/2\Gamma = -0.5$ and $E_{ex}/2\Gamma = 0.25$ (top panel), 0.75 (middle panel), 1.50 (lower panel).

The qualitative behavior of the Andreev states can be easily analyzed in the particular case $E=0$, in which the position of the four states is given by

$$\omega_{\pm}^{\pm} = \pm\Delta \frac{\cos\phi/2 \pm X\sqrt{\sin^2\phi/2 + X^2}}{(X^2+1)}. \tag{14}$$

This expression clearly shows that the effect of a finite exchange field is to split the non-magnetic Andreev states at $\pm\Delta\cos\phi/2$ into four states. The transition to the π junction behavior is associated with the progressive intercrossing of the two ''inner'' bound states. This crossing is illustrated in Fig. 2 for a generic situation. For small exchange field [Fig. 2(a)], the inner states do not cross and the system is in the 0 state. As X increases, the inner states cross at π and thus the current-phase relation exhibits a sign change around $\phi=\pi$. Eventually, when the crossing between the inner states is complete the whole current-phase relation changes sign and the system is in the π state. The state in the intermediate region is conventionally designed as $0'$ or π' depending on the relative stability of the minima of the intercrossing states.

The boundaries between the different regions are straightforwardly obtained from Eq. (13): the curves $X=E$, $X=(E+\sqrt{3+4E^2})/3$, and $X=\sqrt{1+E^2}$ correspond to the 0-$0'$, $0'$-π', and π'-π boundaries, respectively. The full phase diagram of this simple model is illustrated in Fig. 3.

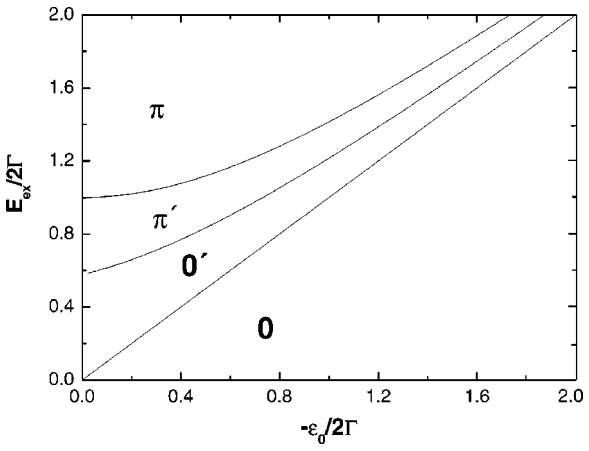

FIG. 3. Phase diagram for the simple model of Sec. III.

IV. ZERO BANDWIDTH LIMIT

A special limit in which the model given by Eq. (1) becomes exactly solvable is the case where the bandwidth of the electrodes tends to zero. This is equivalent to neglect the high-energy excitations in the superconducting electrodes, substituting the frequency-dependent electrodes self-energy by an effective diagonal and nondiagonal level in Nambu space.[25] In this limit the semi-infinite leads connected to the dot are replaced by an effective single site and the terms $H_{L,R}$ describing the leads in Eq. (1) are given by

$$H_{L,R} = \sum_{\sigma} \epsilon_{L,R}\hat{c}^{\dagger}_{L,R\sigma}\hat{c}_{L,R\sigma} + \Delta_{L,R}\hat{c}_{L,R\uparrow}\hat{c}_{L,R\downarrow} + \Delta^{*}_{L,R}\hat{c}^{\dagger}_{L,R\downarrow}\hat{c}^{\dagger}_{L,R\uparrow}. \tag{15}$$

The system thus becomes a sort of ''superconducting molecule'' with a finite number of electron configurations which can be diagonalized exactly. This solution can be useful as a test of the accuracy of the proposed approximations for the infinite system. In spite of its simplicity this limit also gives a qualitative description of the behavior of the full model, as will be shown below.

The exact solution in this limit is obtained by considering electronic configurations with all possible total number of electrons, the pairing interaction connecting configurations that differ in two electrons. The eigenstates can be classified into those arising from even or odd number configurations. In the even case the ground state has zero total spin, while in the odd case the ground state is twofold degenerate corresponding to $S_z = \pm 1/2$.

In Fig. 4 we show the evolution of the ground state energy for the even and odd cases for fixed ϵ_0 and increasing U. As can be observed, in the even case the ground-state energy always exhibits a minimum for $\phi=0$, while in the odd case the minimum appears for $\phi=\pi$. This is to be expected from the fact that the system magnetization is finite in the odd case. For small values of U the even case is more stable for all values of the phase [Fig. 4(a)], while the opposite situation is found for large enough U [Fig. 4(d)]. In the intermediate region [Figs. 4(b) and 4(c)] the even and odd energy

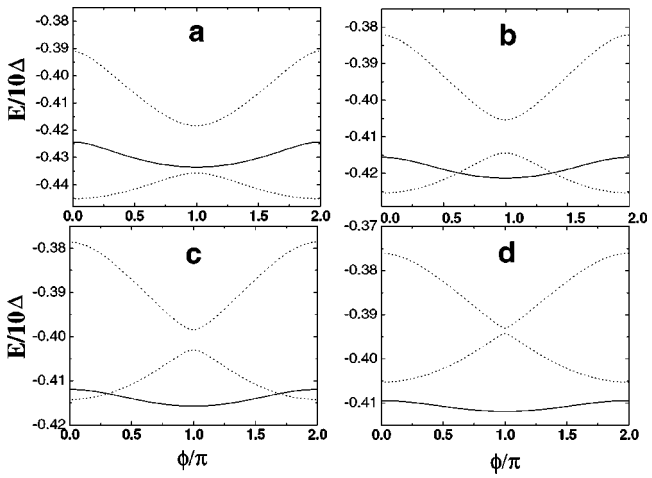

FIG. 4. Energy levels for the model in the zero bandwidth limit with $t_L = t_R = 1.2\Delta$, $\epsilon/\Delta = -10$, and $U/\Delta = 11$ (a), 13 (b), 15 (c), and 18 (d). Dotted and full lines correspond to the even (ground and first excited states) and odd cases, respectively.

levels cross. This level crossing corresponds to the transition between 0 and π junction behavior in the full model. The π state thus corresponds to a situation in which the dot adquires a finite magnetization.

The exact ground-state energy of this simple model can now be used to check the accuracy of the different approximations discussed in Sec. II. For the sake of simplicity we shall restrict this comparison to the $\epsilon_0 = -U/2$ case. In Fig. 5 we show the comparison between the exact, the mean-field and second-order self-energy results for the ground-state energy for different values of U/Δ. At small values of U/Δ [Fig. 5(a)], the energy of the mean-field approximation lies slightly above the exact result both in the nonmagnetic and in the magnetic case. When increasing U/Δ [Fig. 5(b)], the nonmagnetic mean-field solution increasingly deviates from the exact result. In contrast, in the magnetic case, the deviation between the exact and the mean-field solution first increases in the small U range while it progressively decreases for large U. This is due to the fact that the exact ground state corresponds to a localized spin at the central site for $U \to \infty$, which is correctly described by the magnetic mean-field solution.

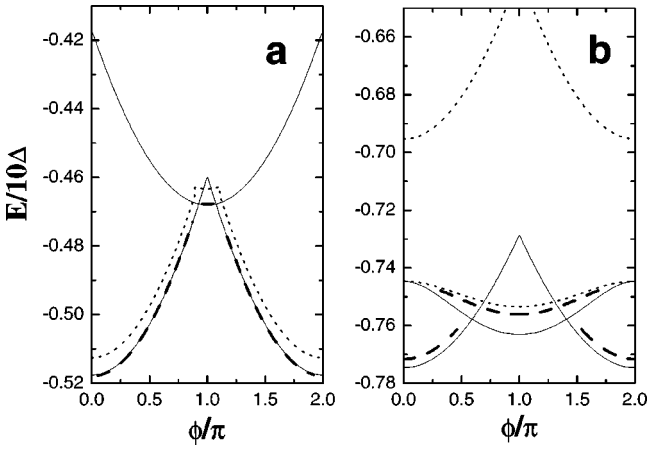

FIG. 5. Comparison of the ground-state energy in the zero bandwidth limit obtained by different approximations: exact diagonalization (full lines), mean-field approximation (dotted lines), and second-order self-energy (dashed lines). The values of the parameters are $\epsilon = -U/2$, $t_L = t_R = 1.2\Delta$, with $U/\Delta = 2.5$ (a) and $U/\Delta = 10$ (b).

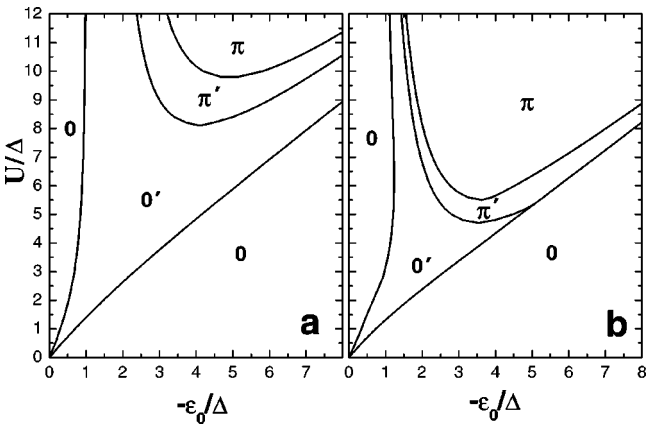

FIG. 6. Phase diagram in the zero bandwidth limit with $t_L = t_R = \Delta$ obtained by exact diagonalization (a) and within the mean-field approximation (b).

The inclusion of the second-order self-energy substantially improves the results of the mean-field approximation both in the magnetic and in the nonmagnetic cases for small and moderate values of U. In the nonmagnetic case the improvement is considerable in the whole range of values of U [Figs. 5(a) and 5(b)]. On the other hand, in the magnetic case the improvement due to the inclusion of correlation effects progressively becomes less important as the mean field tends to the exact solution in the large U limit.

Finally, it is interesting to analyze the phase diagram of the model in the zero bandwidth limit, which turns out to contain the essential features of the full model with the four types of solutions 0, $0'$, π', and π appearing in the previous section. In this discrete model the different phases can be identified by the phase dependence of the ground-state energy.

The exact phase diagram for the zero bandwidth limit is shown in Fig. 6(a). Only the region $U > 0$ and $\epsilon < 0$ is shown as for all other regions the only possible phase is 0 type. Roughly, the π state is found for U/Γ and $-\epsilon_0/\Gamma$ sufficiently large, while the 0 state appears either for U/Γ or $-\epsilon_0/\Gamma$ sufficiently small. The $0'$ and the π' behavior is found in the intermediate regime. It is interesting to notice that for $-\epsilon_0/\Gamma < 1$ and $U/\Gamma \to \infty$ the 0 state is always the more stable. An extrapolation of this result to the full model would imply the absence of π junction behavior in the so-called mixed valence regime, as has been predicted in Ref. 9.

For comparison, the mean-field diagram is also shown in Fig. 5(b). Notice that although the overall behavior is captured in the mean-field solution, correlation effects displace the π region to much larger values of U/Γ and $-\epsilon_0/\Gamma$. Neglecting the induced order parameter in the dot as done in Ref. 8 does not qualitatively change the phase diagram although the full self-consistent solution is somewhat closer to the exact result.

V. RESULTS FOR THE FULL MODEL

The mean-field approximation for the full model has been analyzed in Ref. 8. Although in this work self-consistency in the induced order parameter was neglected, its effects on the total energy is small as already discussed for the zero bandwidth limit. In the present section we will concentrate in discussing the effects of electronic correlations beyond the mean-field solution. We will consider the electron-hole symmetric situation ($\epsilon_0 = -U/2$) in which electron correlation effects are expected to be more important.

For a fixed value of U, the physical behavior of the model is controlled by the dimensionless parameter Δ/Γ. Is is interesting to analyze in detail the two opposite limits $\Delta/\Gamma \gg 1$ and $\Delta/\Gamma \ll 1$

$\Delta/\Gamma \gg 1$ *limit*. This situation corresponds to a dot very weakly coupled to the leads. In this limit the exact solution can be obtained due to the fact that the problem can be mapped into a two-level Hamiltonian describing the dynamics of the Andreev states. This can be shown by first considering the noninteracting ($U=0$) situation. In this case, the spectral density of the dot exhibits bound states at energies $\omega_s = \pm 2\Gamma \cos\phi/2$ and the continuous part becomes negligible. Consequently, the retarded Green function at the dot can be simply written as

$$\hat{G}^r(\omega) \rightarrow \begin{pmatrix} \omega & -\omega_s \\ -\omega_s & \omega \end{pmatrix}^{-1}, \tag{16}$$

indicating that the corresponding effective Hamiltonian is given by $\hat{H}^{\text{eff}} = \omega_s[\hat{c}_\uparrow \hat{c}_\downarrow + \hat{c}_\downarrow^\dagger \hat{c}_\uparrow^\dagger]$. When introducing a finite U, the diagonal level at $-U/2$ is canceled by the Hartree term and the remaining part of the Hamiltonian associated with the Coulomb interaction becomes $U(n_\uparrow - 1/2)(n_\downarrow - 1/2) - U/4$. This term vanishes for the case of an empty and a doubly occupied dot, while it yields an energy $-U/2$ for the single electron case. As a consequence, the ground state of the system is either the symmetric combination of empty and doubly occupied configurations (with energy $-\omega_s$) or the doubly degenerate single occupied state (with energy $-U/2$). Thus, the transition to the magnetic π state takes place when $U/2 > 2\Gamma$.

$\Delta/\Gamma \ll 1$ *limit*. In this opposite limit one would expect to recover gradually the properties of a normal system. In particular, for $U > \Gamma$ the features associated with the Kondo effect should emerge. Figure 7 shows the dot spectral density in this regime for increasing values of U obtained in the second-order self-energy approximation. For comparison the spectral density in the normal state is also shown. As can be observed, the spectral density is similar to the one found in the normal state except for the superimposed features in the gap region. The overall shape evolves as in the normal case from a single Lorentzian broad resonance for $U < \Gamma$ to the three peaked structure characteristic of the Kondo regime when $U > \Gamma$. In this regime the relevant energy scale is set by the Kondo temperature T_K which essentially measures the width of the Kondo resonance in the normal state. Within the second-order self-energy approximation $T_K \sim \Gamma/(1-\alpha_0)$, where $\alpha_0 = (\partial\Sigma/\partial\omega)(0)$. In the symmetric case

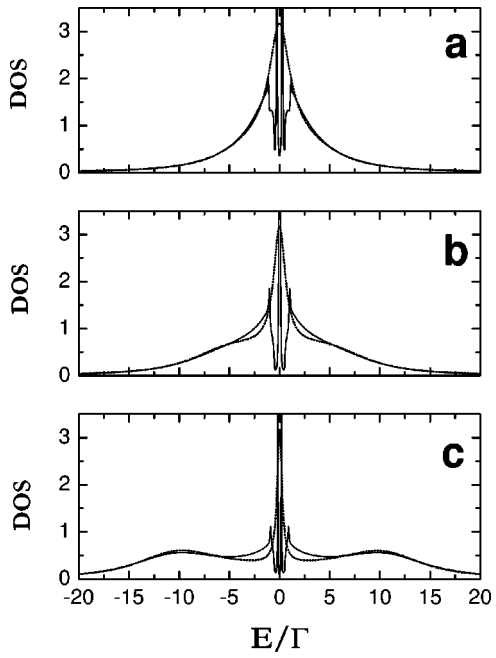

FIG. 7. Density of states for the symmetric case in the regime $\Gamma > \Delta$. The values of the parameters are $\Delta/\Gamma = 0.2$ and $U/\Gamma = 5$ (a), 10 (b), and 20 (c). The dotted lines indicate the corresponding results for the normal state.

$$\alpha_0 = -\left(\frac{U}{2\pi\Gamma}\right)^2 \left(3 - \frac{\pi^2}{4}\right), \tag{17}$$

which coincides with the perturbative result of Ref. 26 for the Anderson model. Although this approach fails to give the exponential decay of the Kondo temperature with U it gives a rather good description of the spectral density in the moderate U/Γ range.[23]

The coexistence of the Kondo and Josephson effects is to be expected as far as $T_K > \Delta$. When U is further increased the system should evolved into the magnetic π state with the suppression of the Kondo effect.

Let us analyze the self-energy in this limit. The effective one-electron problem in this case is characterized by the presence of Andreev states which, from Eq. (11), are located at $\omega_s = \Delta\sqrt{1-\tau\sin^2\phi/2}$, where $\tau = 4\Gamma^2/(\epsilon_{\text{eff}}^2 + 4\Gamma^2)$ is the normal transmission in the effective problem (in the electron-hole symmetric case considered here $\epsilon_{\text{eff}} = 0$ and $\tau = 1$), similar to the case of a single channel point contact. The weight of the Andreev states at the dot site decreases as Δ/Γ according to the expression $\Delta|\sin\phi/2|/4\Gamma$. Also the induced order parameter tends to zero as Δ/Γ in this limit.

The electron self-energy can then be evaluated retaining only terms of order Δ/Γ. The contributions labeled as 11(b) and 21(a) can be altogether neglected as they involve more than one anomalous propagator and are thus of order $(\Delta/\Gamma)^2$. On the other hand, from the general expressions for the second-order self-energy, Eqs. (A1), (A4) in the Appendix, it should be noticed that there are three types of contributions to $\Sigma^{(2)}$: one involving only the discrete part of the one-electron spectral densities, another one involving only the continuous part; and terms in which both the localized

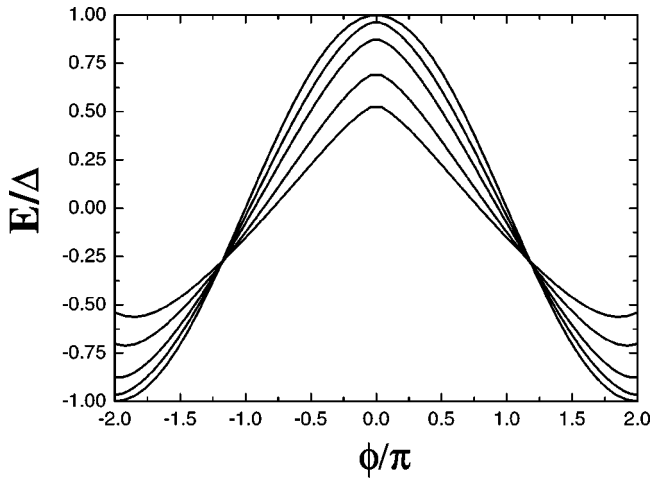

FIG. 8. Renormalized bound states within the gap in the regime $\Gamma \gg \Delta$ with $U/\Gamma = 0$, 10, 14, 18, and 20.

states and the continuous spectrum are mixed. The first of these contributions is of order $(\Delta/\Gamma)^3$ and can be neglected. The resulting expression for $\Sigma^{2)}$ up to first order in Δ/Γ for $|\omega| < \Delta$ is

$$\Sigma_{11}^{(2)}(\omega) \simeq -\left(\frac{U}{2\pi\Gamma}\right)^2 \left(3 - \frac{\pi^2}{4}\right)\omega, \tag{18}$$

$$\Sigma_{12}^{(2)}(\omega) \simeq \left(\frac{U}{2\pi\Gamma}\right)^2 \left[\left|\sin(\phi/2)\right| + 2\left(1 + \frac{1}{\pi}\right)\cos(\phi/2)\right]\Delta. \tag{19}$$

These expressions for the self-energies allow one to determine the renormalization of the states inside the gap due to the interactions. For moderate values of U ($U < 10\Gamma$) the renormalized states have approximately the same phase dependence as in the noninteracting case [i.e., $\sim\cos(\phi/2)$] but with a narrower dispersion given by $\tilde{\omega}_s(0) \simeq \Delta[1 - (U/U_0)^2]$, where $(U_0/\Gamma)^2 = (\Gamma/\Delta)\pi^2/(2\pi + 2)$. For larger values of U the phase dependence of the states starts to deviate from this simple law. This is illustrated in Fig. 8.

The evolution of the renormalized Andreev states indicate that the critical currents are suppressed as $\sim[1 - (U/U_0)^2]$ in this limit (for moderate values of U). One can summarize the results for the full model in the symmetric case by discussing the phase diagram shown in Fig. 9. In this figure we compare the results of the mean-field and the second-order self-energy approximations for the critical U, U_c, defining the transition to the π state. As can be observed both approximations yield the same result in the $\Gamma/\Delta \ll 1$ limit. A close inspection of this regime, illustrated by the inset in Fig. 9, shows that the transition takes place for $U_c \sim 4\Gamma$ when $\Gamma \to 0$ in agreement with the exact result. As Γ/Δ increases the predictions of the two approaches start to deviate. The mean field predicts an almost linear relation between U_c and Γ although with a larger slope than in the $\Gamma \ll \Delta$ limit. On the other hand, the second-order self-energy predicts a faster increase of U_c with Γ. Notice that in the normal state ($\Delta \to 0$) there should be no transition into a magnetic state for

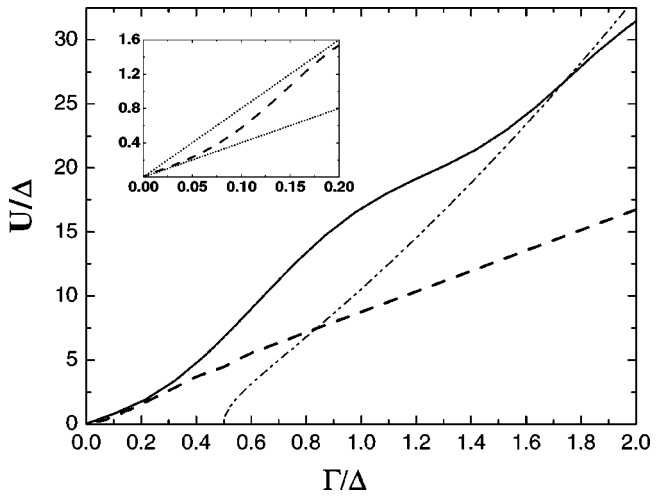

FIG. 9. Phase diagram in the symmetric case for the full model. The full and the dashed lines correspond to the onset of the π state within the second-order self-energy and the mean-field approximation, respectively. The dash-dotted line corresponds to $T_K = \Delta$ within the second-order self-energy approximation. Inset: closer view of the $\Gamma \ll \Delta$ region showing the behavior of the mean-field approximation. The dotted lines indicate the different slopes in the $\Gamma \ll \Delta$ and $\Gamma > \Delta$ regimes.

finite U. We also show as a reference the line where T_K in the normal state, given by the second-order self-energy approximation, matches Δ. It can be observed that the criterium $T_K \sim \Delta$ for the transition to the π state is a rather good for Γ sufficiently large.

VI. CONCLUSIONS AND FINAL REMARKS

We have presented a theoretical analysis of the Josephson transport through a strongly correlated level coupled to superconducting electrodes. The analysis has been specially focused in the effect of electron correlations on the subgap Andreev states. These states determine to a large extent the current-phase relation in this system. The transition to a π state can be understood as a result of the intercrossing of the subgap states induced by an increasing Coulomb interaction. Within this model this transition corresponds to a truly quantum phase transition in which the ground state becomes degenerate having a localized magnetic moment at the dot level as already noticed in Ref. 10. It is worth noticing that this situation cannot exist in the absence of superconductivity. In fact, this behavior can be traced to the suppression of the Kondo effect (in which the electrons at the dot level couple to a singlet) due to the absence of low-energy excitations in the superconducting leads.

In the present analysis we have used different approximation methods. In order to get insight on the behavior of the Andreev states in the transition to the π state we have first analyzed a simple mean-field model in which the electron interactions are represented by a local exchange field. We have also studied the zero bandwidth limit which allows for an exact diagonalization. It has been shown that the study of this limit already illustrates the different types of behaviors that can be found in the full model. These results have also

been used to determine the accuracy of the self-energy approach, showing that it considerably improves the results of the mean-field approximation for moderate values of the Coulomb interaction. Finally, we have presented results for the full model in different regimes. In the limit $\Delta \gg \Gamma$ we have shown that the problem can be solved exactly, its dynamics being described by a two level Hamiltonian corresponding to the Andreev states. On the other hand, for $\Gamma \gg \Delta$ there is a coexistence of Kondo and Josephson effects for $T_K > \Delta$, the main effect of electron correlations being included in a renormalization of the critical current.

The present work constitutes a first step in the study of the transport properties of a quantum dot coupled to superconducting leads in a nonequilibrium situation, i.e., with an applied bias voltage. This would allow one to analyze an experimental situation such as the one of Ref. 3. Work along this line is under progress.

ACKNOWLEDGMENTS

This work has been supported by the Spanish CICyT under contract BFM2001-0150.

APPENDIX

The different contributions to the self-energy represented in Fig. 1 can then be written in terms of the one-electron propagators in the following way:

$$\Sigma^{r(2)}(\omega)_{11,a} = -\frac{U^2}{(2\pi i)^3}\int d\epsilon_1 \int d\epsilon_2 \int d\epsilon_3 \frac{G_{11}^{(0)+-}(\epsilon_1)G_{22}^{(0)+-}(\epsilon_2)G_{22}^{(0)-+}(\epsilon_3) - G_{11}^{(0)-+}(\epsilon_1)G_{22}^{(0)-+}(\epsilon_2)G_{22}^{(0)+-}(\epsilon_3)}{\omega - \epsilon_1 - \epsilon_2 + \epsilon_3 + i0^+}, \tag{A1}$$

$$\Sigma^{r(2)}(\omega)_{11,b} = -\frac{U^2}{(2\pi i)^3}\int d\epsilon_1 \int d\epsilon_2 \int d\epsilon_3 \frac{G_{12}^{(0)+-}(\epsilon_1)G_{21}^{(0)+-}(\epsilon_2)G_{22}^{(0)-+}(\epsilon_3) - G_{12}^{(0)-+}(\epsilon_1)G_{21}^{(0)-+}(\epsilon_2)G_{22}^{(0)+-}(\epsilon_3)}{\omega - \epsilon_1 - \epsilon_2 + \epsilon_3 + i0^+}, \tag{A2}$$

$$\Sigma^{r(2)}(\omega)_{21,a} = -\frac{U^2}{(2\pi i)^3}\int d\epsilon_1 \int d\epsilon_2 \int d\epsilon_3 \frac{G_{21}^{(0)+-}(\epsilon_1)G_{12}^{(0)+-}(\epsilon_2)G_{21}^{(0)-+}(\epsilon_3) - G_{21}^{(0)-+}(\epsilon_1)G_{12}^{(0)-+}(\epsilon_2)G_{21}^{(0)+-}(\epsilon_3)}{\omega - \epsilon_1 - \epsilon_2 + \epsilon_3 + i0^+}, \tag{A3}$$

$$\Sigma^{r(2)}(\omega)_{21,b} = -\frac{U^2}{(2\pi i)^3}\int d\epsilon_1 \int d\epsilon_2 \int d\epsilon_3 \frac{G_{22}^{(0)+-}(\epsilon_1)G_{11}^{(0)+-}(\epsilon_2)G_{21}^{(0)-+}(\epsilon_3) - G_{22}^{(0)-+}(\epsilon_1)G_{11}^{(0)-+}(\epsilon_2)G_{21}^{(0)+-}(\epsilon_3)}{\omega - \epsilon_1 - \epsilon_2 + \epsilon_3 + i0^+}. \tag{A4}$$

Notice that $G^{(0)+-}/2\pi i$ and $G^{(0)-+}/2\pi i$ in the above equations correspond, respectively, to the occupied and unoccupied states in the dot spectral density.

The total self-energy is obtained by adding the contributions labeled by (a) and (b) in the above equations. The remaining self-energy components ($\Sigma_{22}^{r(2)}$ and $\Sigma_{12}^{r(2)}$) are obtained by similar expressions. In the nonmagnetic case the diagonal self-energy components are related by $\Sigma_{22}^{r(2)}(\omega) = -\Sigma_{11}^{a(2)}(-\omega)$. This relation does not hold in the general magnetic case, except when $\epsilon_0 = -U/2$ for which $\Sigma_{11}^{r(2)}(\omega) = \Sigma_{22}^{r(2)}(\omega)$.

[1] D. Goldhaber-Gordon *et al.*, Nature (London) **391**, 156 (1998); S.M. Cronenwett *et al.*, Science (Washington, DC, U.S.) **281**, 540 (1998).
[2] J. Nygard, D.H. Cobden, and P.E. Lindeloff, Nature (London) **408**, 342 (2000); M.R. Buitelaar, A. Bachtold, T. Nussbaumer, M. Iqbal, and C. Schönenberger, Phys. Rev. Lett. **88**, 156801 (2002).
[3] M.R. Buitellar, T. Nussbaumer, and C. Schönenberger, Phys. Rev. Lett. **89**, 256801 (2002).
[4] R. Fazio and R. Raimondi, Phys. Rev. Lett. **80**, 2913 (1998); **82**, 4950 (1999); K. Kang, Phys. Rev. B **58**, 9641 (1998); A.A. Clerk, V. Ambegaokar, and S. Hershfield, *ibid.* **61**, 3555 (2000).
[5] J.C. Cuevas, A. Levy Yeyati, and A. Martín-Rodero, Phys. Rev. B **63**, 094515 (2001).
[6] A. Levy Yeyati, J.C. Cuevas, A. López-Dávalos, and A. Martín-Rodero, Phys. Rev. B **55**, R6137 (1997); G. Johansson, V.S. Shumeiko, E.N. Bratus, and G. Wendin, Physica C **293**, 77 (1997).
[7] S. Ishizaka, J. Sone, and T. Ando, Phys. Rev. B **52**, 8358 (1995).
[8] A.V. Rozhkov and D.P. Arovas, Phys. Rev. Lett. **82**, 2788 (1999).
[9] A.A. Clerk and V. Ambegaokar, Phys. Rev. B **61**, 9109 (2000).
[10] A.V. Rozhkov and D.P. Arovas, Phys. Rev. B **62**, 6687 (2000).
[11] A.V. Rozhkov, D.P. Arovas, and F. Guinea, Phys. Rev. B **64**, 233301 (2001).

[12] I.O. Kulik, Sov. Phys. JETP **22**, 841 (1966).
[13] H. Shiba and T. Soda, Prog. Theor. Phys. **41**, 25 (1969).
[14] L.I. Glazman and K.A. Matveev, Pis'ma Zh. Éksp. Teor. Fiz. **49**, 570 (1989) [JETP Lett. **49**, 659 (1989)].
[15] B.I. Spivak and S.A. Kivelson, Phys. Rev. B **43**, 3740 (1991).
[16] V.V. Ryazanov *et al.*, Phys. Rev. Lett. **86**, 2427 (2001).
[17] L. V. Keldysh, Sov. Phys. JETP **20**, 1018 (1965).
[18] Y. Nambu, Phys. Rev. **117**, 648 (1960).
[19] A. Levy Yeyati, A. Martín-Rodero, and F.J. García-Vidal, Phys. Rev. B **51**, 3743 (1995).
[20] A. Martín-Rodero *et al.*, Solid State Commun. **44**, 911 (1982); A. Martín-Rodero *et al.*, Phys. Rev. B **33**, 1814 (1986).
[21] A. Levy Yeyati, A. Martín-Rodero, and F. Flores, Phys. Rev. Lett. **71**, 2991 (1993); A. Levy Yeyati, F. Flores, and A. Martín-Rodero, *ibid.* **83**, 600 (1999).
[22] H. Kajueter and G. Kotliar, Phys. Rev. Lett. **77**, 131 (1996).
[23] A.C. Hewson, *The Kondo Problem to Heavy Fermions* (Cambridge University Press, Cambridge, 1993).
[24] A. Martín-Rodero, F.J. García-Vidal, and A. Levy Yeyati, Phys. Rev. Lett. **72**, 554 (1994).
[25] I. Affleck, J.S. Caux, and A.M. Zagoskin, Phys. Rev. B **62**, 1433 (2000).
[26] K. Yamada and K. Yosida, Prog. Theor. Phys. **53**, 1286 (1975).